AN ESTIMATION OF THE PASSIVE PRESSURE AGAINST INTEGRAL BRIDGE ABUTMENTS CONSIDERING ARCHING EFFECTS

MOJTABA MOVAHEDIFAR and JAFAR BOLOURI BAZAZ

about the authors

corresponding author
Mojtaba Movahedifar
Department of Civil Engineering,
Neyshabur Branch, Islamic Azad University
Neyshabur, Iran
E-mail: m.movahedi@iau-neyshabur.ac.ir

Jafar Bolouri Bazaz
Department of Civil Engineering,
Ferdowsi University of Mashhad
Mashhad, Iran
E-mail: bolouri@um.ac.ir

Abstract

Most civil engineering structures are subjected to cyclic loading during their service life, such as retaining walls, wave loading on offshore structures, seismic loading and the traffic loading of pavements. In the case of an integral abutment bridge (IAB), as an example, the backfill granular material is subject to slow cyclic stress and strain changes under drained conditions. These bridges are constructed so that the top deck is longitudinally continuous. In other words, IABs are joint-less bridges where the superstructure is connected with the abutment. The rigid connection enables the abutment and superstructure to act as a single structural unit, i.e., the expansion joints which are widely used in traditional bridges are removed in IABs. This removal is mainly due to the high costs of maintenance. The behavior of IABs is dominated by the cyclical temperature changes in the bridge deck. This results in the imposition of cyclical horizontal displacements to the backfill soil of the abutments. The present research is an effort to investigate the induced passive pressure on the IABs, using a laboratory model and an analytical approach. The results indicate that the passive pressure distribution is non-linear and its maximum value along the wall is dependent on the magnitude of the wall rotation and number of cycles. It seems that there are two different mechanisms for this behavior. In the above part of the wall, sand behaves as a plastic material. A decline in the passive pressure in the bottom part, however, is the result of arching.

keywords

integral abutment bridge, cyclic displacement, passive pressure, arching

1 INTRODUCTION

Integral abutments bridges can be categorized into three types: shallow abutments, full height frame abutments on spread footings, and full height embedded abutments. Shallow abutments and frame abutments (Fig. 1.a) normally retain granular backfill. Embedded abutments are typically constructed in-situ in clayey ground (Fig. 1.b) [1].

The abutment of the integral bridges is generally subjected to cyclic displacement. This is due to the omission of the joint between the deck and the abutment, i.e., the superstructure is connected monolithically with the abutment [2-6]. This rigid connection enables the abutment and the superstructure to act as a single structural unit, and ensures full moment transfer between the abutment and the slab [5]. The omission of the expansion joints results in a fluent traffic and reduces the maintenance costs [7, 8].

The behaviour of these structures is dominated by the cyclical temperature changes in the bridge deck. In other words, due to the daily and seasonal variations in temperature, the bridge deck experiences the movement of thermal expansion and contraction, resulting in the imposition of cyclical horizontal displacements to the backfill soil of the abutments [9], and this imposed cyclic movement will in turn cause changes in the behaviour of the backfill material behind the bridge abutment.

The most influential lateral loading on integral bridges is due to the daily and seasonal thermal expansions and contractions of the superstructure [5].

In these bridges, if the variation in the environment temperature and the coefficient of thermal expansion of

the bridge are δ_{TEB} (ºC) and α_t (1/ºC), respectively, the change in the length of the bridge due to temperature changes, d_0, can be calculated as [3-5]:

$$d_0 = \alpha_t . \delta_{TEB} . L \qquad (1)$$

in which L is the length of the bridge deck (Fig. 1).

In practice, the soil at the back of the bridge abutment would resist against the deck elongation. The actual bridge deck elongation is, therefore, less than d_0. Dicleli showed that the actual bridge-deck elongation, d', could be calculated as (Fig. 1):

$$d' = d_o - d_c \qquad (2)$$

In this relation, d_c is the amount of deck contraction due to the backfill material's resistance [10]. Obviously,

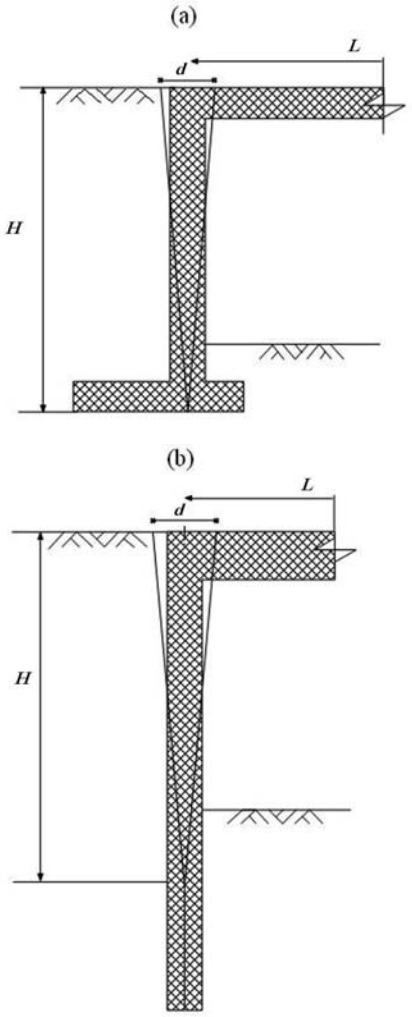

Figure 1. Imposed cyclic movement of the bridge deck to the retaining wall.

d_c depends on the bridge's axial stiffness. However, the effect of the backfill soil resistance on the behaviour of the abutment wall's movement is mostly neglected [11].

The effect of the soil-structure interaction of the integral bridges has been an interesting issue for many investigators. A wide range of experimental researches deals with investigations of the induced lateral earth pressure due to the cyclic movement of the bridge deck [1, 9, 12-19].

Springman et al., for example, performed a series of tests on a smooth and rigid wall that had the ability to rotate around a hinge located at its bottom. The induced stress on the face of the wall was measured using miniature pressure transducers. Their results indicate an increase in the maximum lateral earth pressure due to cyclic movements [18].

Barker and Carder performed a series of in-situ tests in which the pressure escalation was measured behind a bridge abutment. The length of the bridge was 40 m and the lateral movement and the stress behind the bridge abutment were evaluated. They observed a trend of pressure increase during the daily and seasonal temperature variations. Again, they evaluated the stress variations of a bridge abutment with a length of 50 m. The pressure and the movement of the abutment were recorded during the construction and the first year of operation. The results indicate that the lateral earth pressure during construction was about the at-rest pressure and gradually increased afterwards [13]. In addition, investigations indicate that the lateral earth pressure distribution is nonlinear and reaches its maximum value near the middle of the abutment [12]. More investigations indicate that the stress increases initially with depth and then decreases gradually in the region adjacent to the bottom of the wall. This phenomenon can be well interpreted by arch forming in this region. Many researchers have reported the stress reduction due to the arching effect [9, 17, 20-23].

The main objective of this paper is to investigate the influences of cyclic rotation on the behaviour of sandy soil behind the shallow abutment and frame abutments. To investigate these effects, a laboratory retaining wall was introduced. In this model, the wall itself was made from hard plastic material and stiffened by backing alloys in order to be sufficiently rigid.

Since the integral bridge abutments are generally analysed in the plane strain condition [1, 24], and in practice, the abutment is mostly built in reinforced concrete, it is relatively rigid [11], this is the reason that the retaining wall model was designed in such a way as to maintain the plane strain condition.

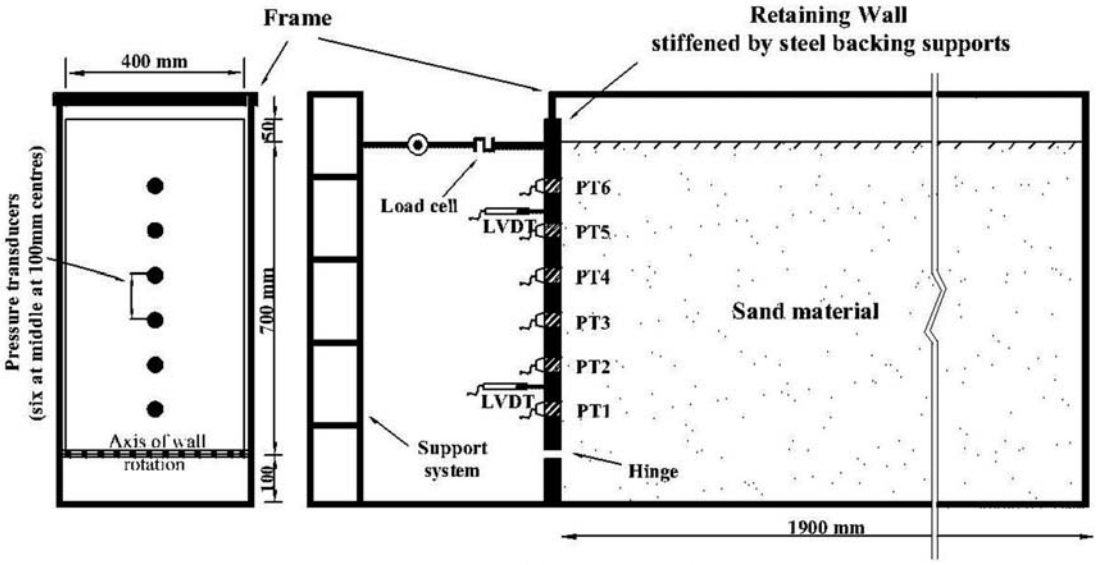

Figure 2. A schematic view of the retaining wall model apparatus.

The granular material placed behind any abutment is normally specified to be in a dense condition, achieved by mechanical compaction [25]. However, loose granular backfill has also been recommended behind the integral abutments as a possible means of avoiding high earth lateral pressures [25]. In this paper, the behaviour of sandy materials is loose conditions. The details of the model test, the loading condition and the material properties are presented in the following sections. Also, in order to interpret the laboratory model test results, an analytical model has been developed and the test results have been compared and validated.

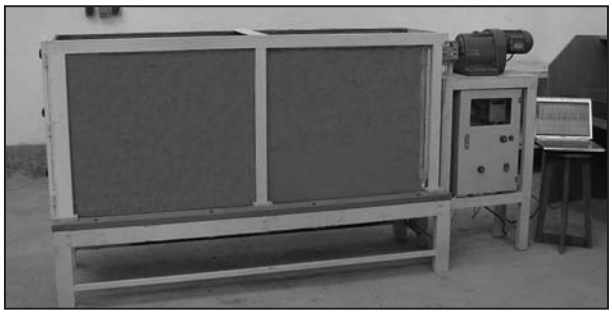

Figure 3. A general view of the laboratory model.

2 THE LABORATORY MODEL

In practice, the behaviour of the integral bridge abutment is in the plane strain condition [1, 24]. To maintain this condition in the laboratory model, the glassy sidewalls (wing walls in practice) were fixed inside a frame. This prevented the lateral movement of sidewalls. It, in turn, results in the plane strain conditions to be maintained. In the laboratory model, the frame was made from steel with glass panels. Fig. 2 illustrates a schematic presentation of the apparatus. In order to observe the soil deformation during the tests, both longitudinal sides of the apparatus were made from thick (10 mm) glass panel. Shown in Fig. 3 is a general view of the laboratory model. The experimental device is 400 mm in width and 850 mm in height, allowing soil to be filled up to a depth of 800 mm. In this model, the rigid retaining wall itself was made from a hard plastic material and stiffened by backing alloys. It was able to rotate around its toe by a hinge, which was installed in 100 mm, measured from the bottom of the apparatus. This resulted in up to 700 mm of soil depth to be contributed in the test. The friction between the wall and the glass panels was minimized by using PTFE sealing strips. In this model, the length of the apparatus was long enough to allow the rupture surface to be formed wholly. Based on the maximum friction angle of the backfill sand, which measured about 38.2º (Table 1), and assuming a plane rupture surface with an angle of $(45+\phi/2)^0$ with respect to the vertical, the length of the apparatus, l, was calculated as:

$$l=H.\tan(45+\phi/2)= 700\times\tan(45+38.2/2)\approx 1450 \text{ mm} \quad (3)$$

Since the rupture surface is not completely plane and tends to be curvature, the length of the laboratory model was increased to 1900 mm. The friction angle between the sand and the wall was measured using direct shear test. Due to the smoothed face of the wall, the friction angle

between the walls and the sand, which was measured by direct shear device, was very low and close to zero. The lateral soil pressure measurements were made on the face of the wall using pressure transducers with a flat diaphragm that was very sensitive to the pressure. Six pressure transducers, PT1 to PT6, are installed at heights of H=20, 30, 40, 50, 60 and 70 cm, measured from the bed of the sand reservoir. These transducers measure the stress perpendicular to their face (i.e., the lateral earth pressure). The exact installation position of the pressure transducer on the rotatable wall is also shown in Fig. 2.

In this model, the top of the wall displacement is achieved using a mechanical motor. The driving shaft of the motor provides an inward and outward displacement to simulate the cyclic deformation. The model wall was equipped with a load cell to measure the applied load to the rotatable wall. This facilitated controlling the equilibrium of the applied load and the lateral earth pressure distribution on the wall face. In addition, the horizontal movements of the wall were captured using two LVDTs, installed both at the top and at the middle of the wall (Fig. 2). This made it possible to measure the horizontal movement of the wall and control its rigidity during the test. The reading of these LVDTs showed no wall bending in any test.

All the required data, including the wall displacement, soil pressures, and the applied loads, were captured as signals, using a data acquisition system. The data was then converted into digital numerical values based on calibration sheets.

3 BACKFILL MATERIAL PROPERTIES AND TEST PROGRAM

In the current research Firooz–Kouh sand with a similar texture to Leighton Buzzard sand was used. This sand, with a mean particle size (D_{50}) of 0.55 mm and a uniformity coefficient of 1.425, was employed in the experiments. The friction angle, ϕ, of this sand and the friction angle between the sand and the wall using triaxial and direct shear tests, respectively. Due to the smoothed face of the wall, the friction angle between the walls and the sand, which was measured by direct shear device, was very low and close to zero. In addition, since the purpose of this study is to investigate the behaviour of sandy materials in loose conditions, the sand was rained from a constant drop height of 100 mm. This resulted in an initial sand relative density of 27±2% and unit weight of about 13.92 (kN/m^3). The corresponding internal friction angle was ϕ_{ini} =32.5º. Table 1 summarizes the properties of this sand.

Table 1. Specifications of Firooz-Kough sand.

Friction angle	ϕ_{max}	38.2º
	ϕ_{min}	30.0º
	ϕ_{ini}	32.5º
Void ratio	e_{min}	0.707
	e_{max}	1.040
	e_{ini}	0.95
Unit weight	γ	13.92(kN/m^3)
Grain density	γ_s	26.58(kN/m^3)
Relative density	D_r	27±2%
Specific gravity	G_s	2.71

4 TEST PROGRAM

In the present research, a wide range of experimental tests were carried out. Since the main objective of these series of tests was to evaluate the influence of the large amplitude [26] of wall rotation on the soil-wall interaction, the different amplitudes of the displacement at the top of the wall including $d/2$=1.75,2.45 and 6.50 mm, equivalent to the wall rotation ($d/2H$) of 0.25, 0.35 and 0.929%, are considered for these series of tests.

In these tests the retaining wall (totally smooth) was fixed in the vertical position and the LVDTs were set at zero. The subsequent readings indicated the forward and backward movements of the wall and these movements are repeated in the subsequent cycles.

These tests were terminated when no significant changes in the magnitude and distribution regime of passive pressure were observed. In addition, as we know, the rate of wall abutment of the integral bridges is significantly low (daily and seasonal variations of temperature). Movahedifar and Bolouri-Bazaz have shown the rate of wall movement (for low velocity magnitude) has no significant effect on the passive pressure magnitude [17]. Therefore, in these series of tests, the top of the wall movement velocity was constant and very low (0.015 mm/s). Fig. 4 depicts the induced passive pressure on the face of the wall for different wall movements including $(d/2)_{max}$=1.75, 2.45 and 6.50 mm.

When the test terminated, the settlement profile of the soil layers at different heights was determined by measuring the difference between the coloured sand layers and horizontal lines drawn initially on the glass panel. The settlement profiles for $(d/2)_{max}$=1.75 mm and 2.45 mm, for example, are shown in Fig. 5.

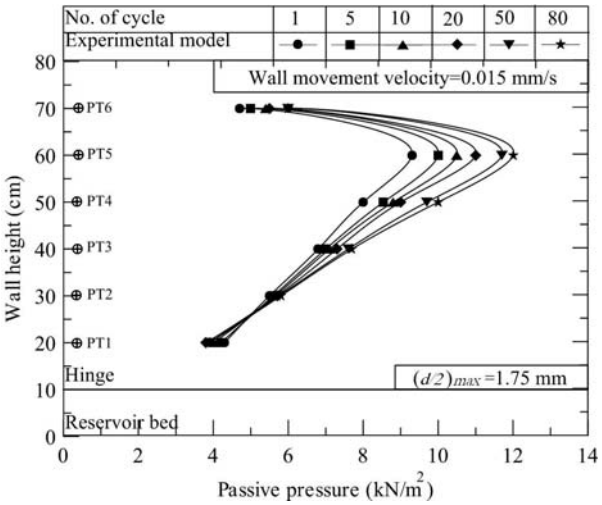

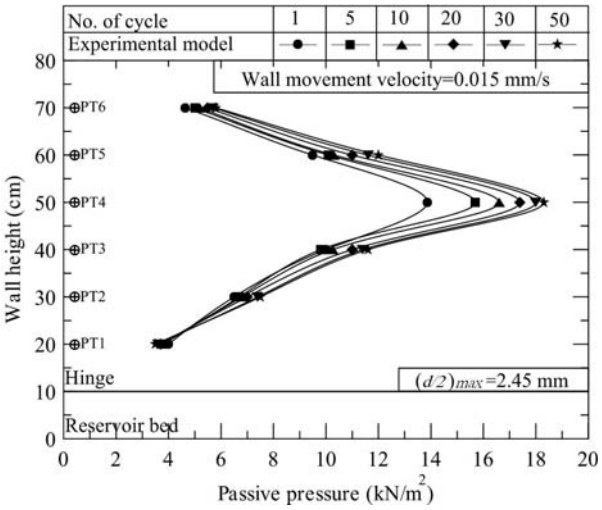

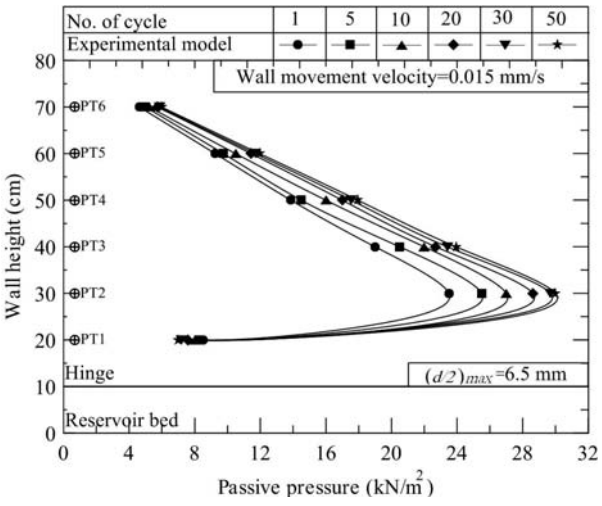

Figure 4. Induced passive pressure on the wall for different top of the wall movements.

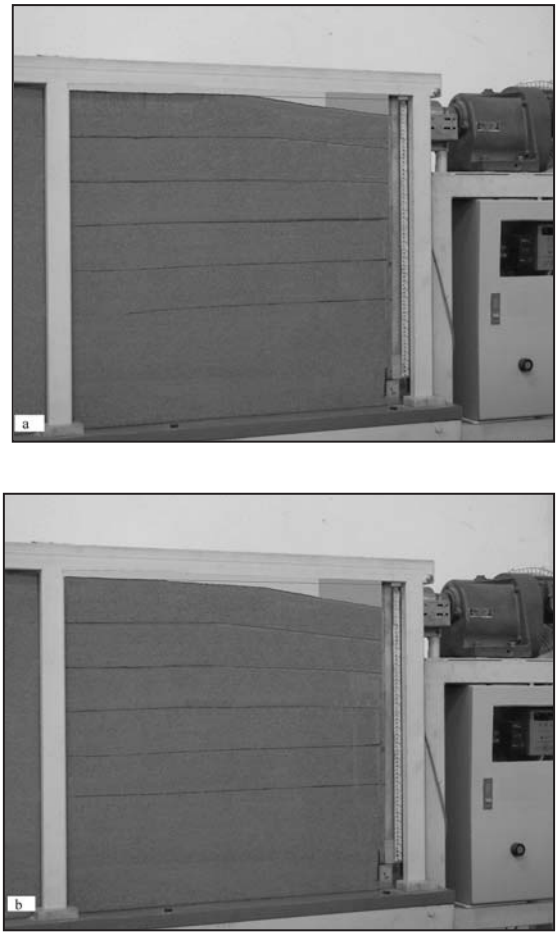

Figure 5. View of the settlement of the sand layers in the final cycles; a: $d/2$=1.75 mm and b: $d/2$=2.45 mm.

The settlement profile shown in Fig.5 is quantified and shown in Fig.6. This figure shows the settlement profiles in the vicinity of the rigid wall for $(d/2)_{max}$=1.75 mm (after 80 cycles), 2.45 mm (after 50 cycles) and 6.5 mm (after 50 cycles). This clearly indicates a huge decrease in void ratio of sand just close to the wall.

The following observations are based on Fig. 4, Fig. 5 and Fig. 6:

- The passive pressure distribution that is non-linear can be divided into two parts: above and below of the maximum point (see Fig. 4). It seems that the sand behaviour is different in these two parts. In the upper part the sand behaviour is plastic. In the lower part, however, a reduction in pressure can be observed. This imitates an arch formation, which tolerates some weight of sand. This results in a reduction in the vertical pressure and this, in turn, causes a reduction in the horizontal pressure.

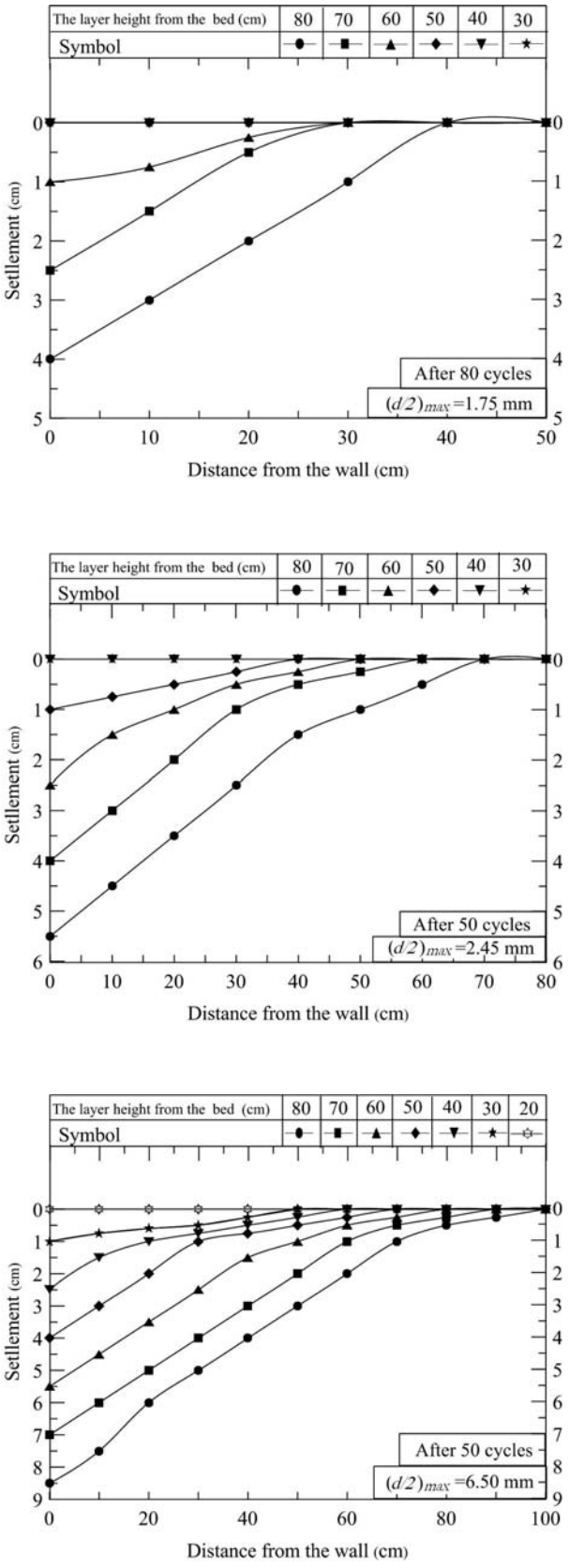

Figure 6. The settlement profile of the sand layers.

– The settlement profiles, shown in Fig. 6, indicate with increasing displacement amplitude, that more layers of soil are affected by the settlement. The heights of the sand layer measured from the top of the wall influenced by the settlement are 20, 30, and 50 cm for the range of 1.75, 2.45, and 6.50 mm displacements, respectively. The soil layers beyond these heights are not affected by the huge settlement on top of the wall. This is a clear indication of a reduction in the voids ratio and an increase in the friction angle in the upper part.

5 ESTIMATION OF THE ARCH ZONE

As shown in Fig. 4, when the wall is pushed inward to the fully passive condition, with an increase in the wall rotation amplitude, the passive pressure reaches a maximum value, after which it decreases gradually. This clearly indicates a decrease in the surcharge, i.e., a decrease in the vertical stress in the bottom part. This reduction is due to the arch forming between the wall and the material, leading to a reduction in the lateral passive pressure as well. If the wall starts to move back, the formed arch is suddenly destroyed, and the vertical stress and horizontal pressure in turn, must be increased. To investigate the process of arch formation, the variations of the passive pressure and the different magnitudes of the wall rotation are illustrated in Fig. 7. In this section, the wall starts from the at at-rest condition (vertical position), and then the wall is pushed inward to the fully passive condition. It is then pulled back to the fully active condition and returned to the initial position.

The data taken from six pressure transducers, PT1 to PT6 (Fig. 2), are shown in Fig. 7. It should be noted that the captured data are pertained to the first half of a cycle, i.e., from at rest to the passive condition and just after retuning back to the initial position.

Fig. 7 indicates for $(d/2)_{max}$ =1.75, 2.45 and 6.5mm, when the wall resumes to move back, the pressure in the transducers PT1 to PT4 [for $(d/2)_{max}$= 1.75 mm] and PT1 to PT3 [for $(d/2)_{max}$= 2.45 mm] and finally just PT1 [for $(d/2)_{max}$= 6.5 mm] is increased and no significant increase for the remaining pressure transducers is observed. This means that with moving back the wall, the arch forming is destroyed, which results in an increase in the vertical stress. This, in turn, causes the lateral pressure to increase as well. In addition, it can be deduced that with increasing wall rotation amplitude, the height of the arch zone moves down. It is thought that if the wall rotation increases further (which is out of the

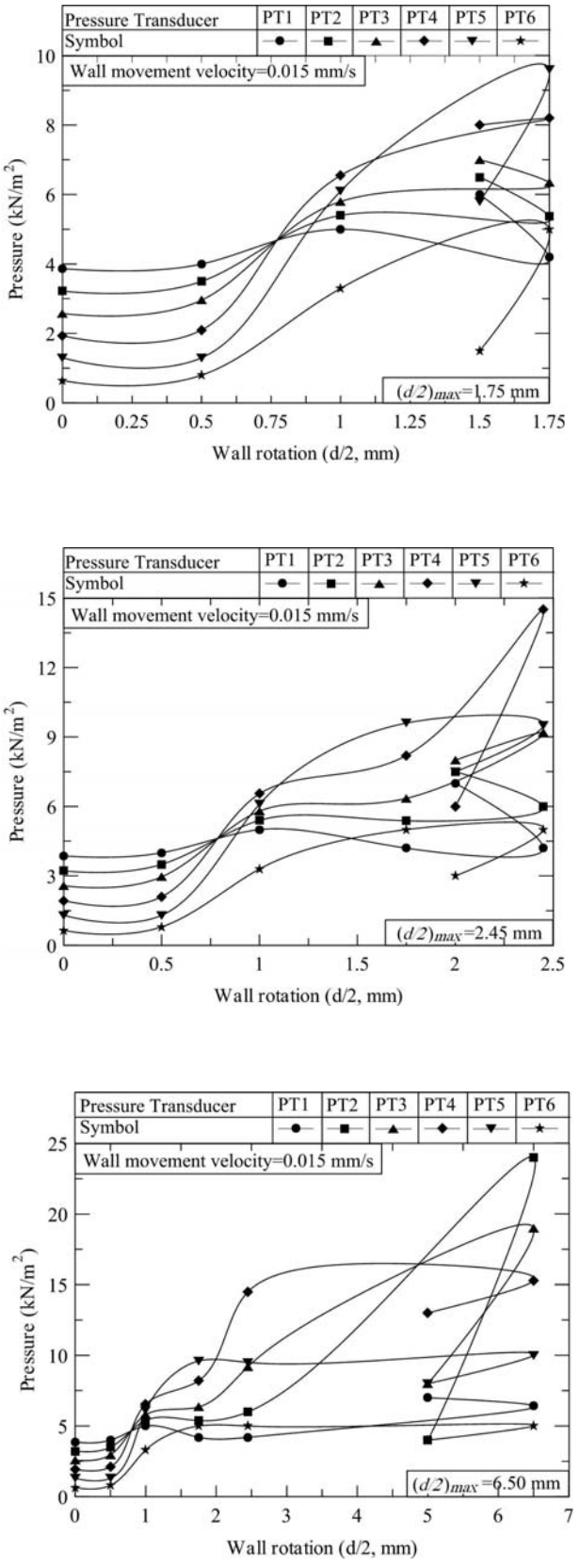

Figure 7. Passive pressure measured at various depths.

working range of the laboratory model) a fully passive condition is reached, i.e., the arch forming is (totally) destroyed. It is necessary to mention that the results for more cycles are similar to the first cycle, and that is why the results are reported only for the first cycle.

6 ANALYTICAL APPROACH FOR AN ESTIMATION OF THE PASSIVE PRESSURE

Although a wide range of experimental researches deals with investigations of the induced lateral earth pressure, regarding the cyclic movement of the bridge's deck, it is difficult to have an exact estimation of the passive pressure for IABs. In this section, based on an analytical approach, we attempt to estimate the passive pressure for shallow abutments and frame abutments.

It is known that the rupture surface in rigid retaining wall, rotating about a hinge located in the bottom of the wall, is mainly dependent on the friction between the wall and the soil. The rupture surface, however, is planar for the frictionless wall and curvature in the friction presence [21, 27, 28].

In addition, experimental and theoretical researches indicate that in active and passive conditions the soil failure wedge does not always cross the hinge. The height of the failure wedge depends on the wall rotation amplitude and with the increase in the rotation amplitude, the position of the bottom of the failure wedge approaches to the hinge [29, 30].

Based on the above observations, in order to interpret the interaction behaviour between the soil and the wall, a rigid retaining wall with a height of H is considered (Fig. 8). This wall, which is frictionless (friction angle between the walls and sand was very low and close to zero), is capable of rotating around a hinge located at the bottom of the wall. It is assumed that the failure wedge is forming at the height of H_P (from the top of the wall, Fig. 8) when the wall position is altered from the vertical position to the passive condition.

The angle of this failure wedge with the horizon is assumed to be θ. Consider the soil element ABCD in this wedge, which is called plastic zone. Also consider another soil element, EFGH, in the lower part of the wall with a height of He (the height of the arch zone), for which no failure wedge is formed. This element is located between the wall and a plane which forms an angle μ with the horizon and passes through the hinge. The formation of this hard bounding plane has also been reported by Tsang et al [9].

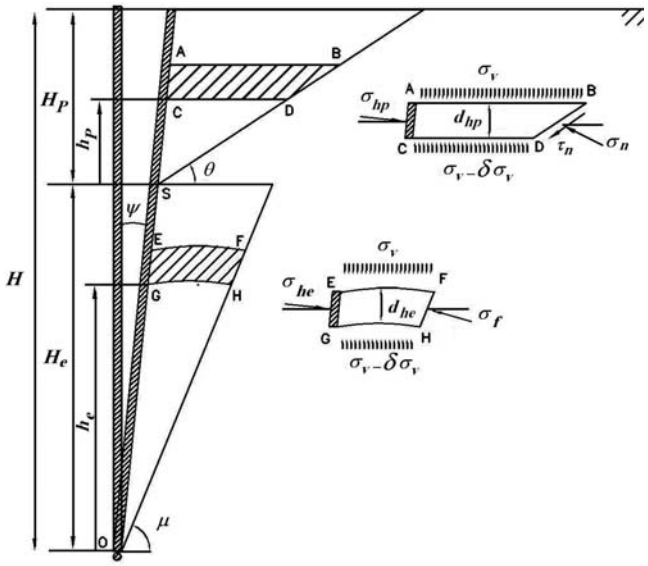

Figure 8. Wall analytical model.

Now, if we write the equilibrium equation for the element ABCD, we have:

$$\sigma_{hp}.\cos\psi.AC-\sigma_n.BD.\cos(\frac{\pi}{2}-\theta)-\tau_n.BD.\cos\theta=0 \quad (4)$$

and:

$$\begin{aligned}&\sigma_{hp}.\sin\psi.AC+\sigma_v.AB-(\sigma_v-\delta\sigma_v).CD\\&+[(CD-AC.\sin\psi)+BD.\cos\theta]\gamma.d_{hp}\\&+\frac{1}{2}\gamma d_{hp}.AC.\sin\psi-\frac{1}{2}\gamma d_{hp}.BD.\cos\theta\\&-\sigma_n BD\sin(\frac{\pi}{2}-\theta)+\tau_n.BD.\sin\theta=0\end{aligned} \quad (5)$$

Also, the following equations can be established for the SAB and SCD triangles and the element ABCD:

$$AC=d_{hp}/\cos\psi \quad (6)$$

$$BD=d_{hp}/\sin\theta \quad (7)$$

$$AB=(hp+d_{hp}).\tan(\frac{\pi}{2}-\theta)-(hp+d_{hp}).\tan\psi \quad (8)$$

$$CD=hp.\tan(\frac{\pi}{2}-\theta)-hp.\tan\psi \quad (9)$$

By substituting these equations into equations 4 and 5 we have:

$$\sigma_{hp}.d_{hp}-\sigma_n.d_{hp}-\tau_n.d_{hp}.\cot\theta=0 \quad (10)$$

The relationship between the shear and the normal stresses in the upper part of the wall and in the element ABCD can be stated as [31]:

$$\tau_n=\sigma_n.\tan\varphi \quad (12)$$

Since equation 12 is valid in the plastic zone, by substituting equations 10 and 12 in equation 11 and ignoring (d^2_{hp}) and after simplification we have:

$$\sigma_{hp}=\frac{(\cot\theta-\tan\psi)(\sigma_v+\delta\sigma_v/d_{hp}.hp+hp.\gamma)}{\left(\frac{\cot\theta-\tan\varphi}{1+\tan\varphi.\cot\theta}-\tan\psi\right)} \quad (13)$$

Also, according to equations 14 and 15, the vertical stress and its variations can be calculated as:

$$\sigma_v=(H-H_e-hp).\gamma \quad (14)$$

$$\partial\sigma_v/d_{hp}=-\gamma \quad (15)$$

Substituting equation 14 and 15 into equation 13 leads to:

$$\sigma_{hp}=\sigma_v.\frac{(\cot\theta-\tan\psi)}{\left(\frac{\cot\theta-\tan\varphi}{1+\tan\varphi.\cot\theta}-\tan\psi\right)} \quad (16)$$

In which *Kp* is the passive lateral earth pressure coefficient, i.e.:

$$Kp=\frac{(\cot\theta-\tan\psi)}{\left(\frac{\cot\theta-\tan\varphi}{1+\tan\varphi.\cot\theta}-\tan\psi\right)} \quad (17)$$

Fig. 9 illustrates a comparison of the above (*Kp*) and the Coulomb passive lateral earth pressure coefficient (*Co*) for the condition of $\delta=\alpha=0^0$, $\omega=(\psi+90)°$ and $\theta=(45-\phi/2)°$. It can be deduced by increasing the wall rotation; the difference becomes greater and greater, especially when the sand friction angle is relatively high. However, as seen in Fig. 9, even for $\phi=45^0$ and $\psi=10^0$ the maximum difference reaches up to about 6.5 percent.

Also, at the lower part of the wall, by writing the equilibrium for the element EFGH, we have:

$$\sigma_{he}.EG.\cos\psi=\sigma_f.FH.\cos(\frac{\pi}{2}-\mu) \quad (18)$$

$$\begin{aligned}&\sigma_{hp}.d_{hp}.\tan\psi+\sigma_v[(hp+d_{hp}).\tan(\frac{\pi}{2}-\theta)-(hp+d_{hp}).\tan\psi]-(\sigma_v-\delta\sigma_v)(hp.\tan(\frac{\pi}{2}-\theta)-hp.\tan\psi)+\\&[hp.\tan(\frac{\pi}{2}-\theta)-hp.\tan\psi-d_{hp}.\tan\psi+d_{hp}.\cot\theta].\gamma.d_{hp}+\frac{1}{2}\gamma.\tan\psi.d^2_{hp}-\frac{1}{2}\gamma.d^2_{hp}.\cot\theta-\\&\sigma_n.d_{hp}.\cot\theta+\tau_n.d_{hp}=0\end{aligned} \quad (11)$$

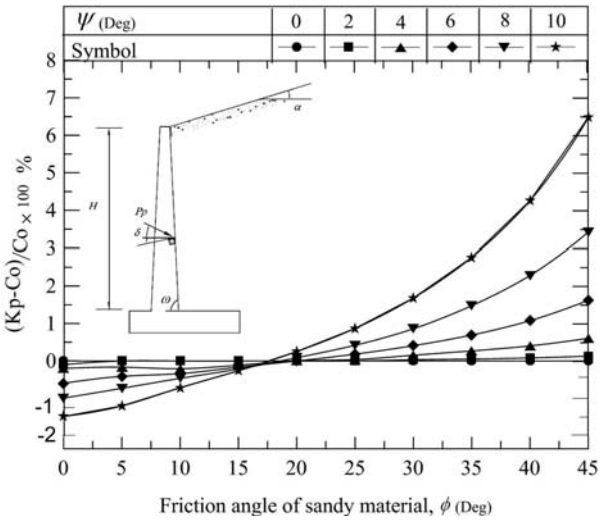

Figure 9. Comparison between the Coulomb coefficient (*Co*) and equation 17 (*Kp*).

$$\sigma_v.EF-\left(\sigma_v-\delta\sigma_v\right).GH+\gamma.d_{he}.GH-\gamma.EG.\sin\psi.d_{he}/2 +\gamma.FH.\cos\mu.d_{he}/2+\sigma_{he}.EG.\sin\psi-\sigma_f.FH.\sin\left(\pi/2-\mu\right)=0 \quad (19)$$

Also, in the element EFGH and the triangles OGH and OEF we have:

$$OG.\cos\mu=OH.\sin\mu=he \quad (20)$$

$$EG.\cos\psi=FH.\cos(\frac{\pi}{2}-\mu)=d_{he} \quad (21)$$

$$GH=OH.\cos\mu-OG.\sin\psi \quad (22)$$

$$EF=OH.\cos\mu-OG.\sin\psi-GE.\sin\psi+FH.\cos\mu \quad (23)$$

By substituting equations 18, 20, 21, 22 and 23 into equation 19, and after some simplification, the following equation is obtained.

$$\begin{aligned}&\sigma_v.\left(he.\cot\mu-he.\sin\psi/\cos\mu-d_{he}.\tan\psi+d_{he}.\cot\mu\right)\\&\quad-\left(\sigma_v-\partial\sigma_v\right).\left(he.\cot\mu-he.\tan\psi\right)+\\&\quad\sigma_{he}.d_{he}.\tan\psi+\gamma.d_{he}.\left(he.\cot\mu-he.\tan\psi\right)\\&-\gamma/2.d^2{}_{he}.\tan\psi+\gamma/2.d^2{}_{he}.\cot\mu-\sigma_{he}.d_{he}.\cot\mu=0\end{aligned} \quad (24)$$

If we ignore ($d^2{}_{he}$) and after the simplification, the following equation is obtained:

$$\begin{aligned}&\sigma_v.\left(\cot\mu-\tan\psi\right)+\partial\sigma_v/d_{he}.he.\left(\cot\mu-\tan\psi\right)\\&+\gamma.he.\left(\cot\mu-\tan\psi\right)-\sigma_{he}.\left(\cot\mu-\tan\psi\right)=0\end{aligned} \quad (25)$$

Obviously, the arching phenomenon decreases the vertical stress. For the upper part of the wall no arching is formed, but for the lower part where the arch exists (Fig. 7), however, the vertical stress reduces and can be stated with the following relation:

$$\sigma_v=\left(H-he\right).\gamma.\beta \qquad 1\geq\beta\geq0 \quad (26)$$

β is a reduction coefficient and is considered to be a function of *he* (equation 27). It is always smaller than unity. For *he*=*He*, however, where the plastic zone starts, β=1.

$$\beta=f\left(he\right) \quad (27)$$

If we derive σ_v (equation 26) with respect to *he* is calculated we have:

$$\partial\sigma_v/d_{he}=H.\gamma.\partial\beta/d_{he}-\left(\gamma.\beta+\gamma.he.\partial\beta/d_{he}\right) \quad (28)$$

By substituting equation 28 and equation 26 into equation 25 and after simplification equation 29 is obtained.

$$\sigma_{he}=H.\gamma.\beta+\gamma.he-2\beta.\gamma.he+\partial_\beta/d_{he}.he.\gamma.\left(H-he\right) \quad (29)$$

Equation 29 shows the horizontal stress in the lower part of the wall. With dividing σ_{he} (equation 29) to σ_v (equation 26), the lateral earth pressure coefficient in the lower part of the wall (*Ke*) can be calculated, i.e.:

$$Ke=\frac{H.\gamma.\beta+\gamma.he\left(1-2\beta\right)}{\left(H-he\right).\gamma.\beta}+\partial\beta/d_{he}.he/\beta \quad (30)$$

Now, for *he*=0, (i.e., at the lowest part of the wall) *Ke*=1. In addition, Tsang et al. considered a linear variation for the lateral earth pressure coefficient in the lower part [9]. With this assumption, *Ke* (equation 30) increases from unity (at the lowest part of the wall) and approaches to *Kp* (at the start of plastic zone; equation 17). Therefore, we have:

$$Ke=1+he.n.\left(Kp-1\right)/H \quad (31)$$

in which *n*=*H*/*He*.

With a comparison of equations 30 and 31 and after simplification we have:

$$\partial\beta/d_{he}=\beta.n.\left(Kp-1\right)/H+\beta/he-\frac{H.\beta+he.\left(1-2\beta\right)}{he.\left(H-he\right)} \quad (32)$$

With the proper integration and by applying the boundary condition of *he*=*H*/*n*=*He*, β=1, equation 33 leads to:

$$\begin{aligned}&\beta=\left(-1/\left(Kp-1\right)/n\right).H.\exp\left(-n.he.\left(Kp-1\right)/H\right)\\&-\exp\left(1/H.n.he.Kp\right)/\exp\left(n.he/H\right)/\left(he-H\right).\\&H.\left(Kp.n-Kp-n\right)/\exp\left(-1\right)/n/\exp\left(Kp\right)/\left(Kp-1\right)\end{aligned} \quad (33)$$

By substituting equations 32 and 33 into equation 29, the lateral earth pressure on the lower part of the wall can be calculated. Now, for specific values of ψ and ϕ, according to equations 16 and 29, the lateral earth pressure on the upper and lower parts can be calculated.

Now, based on an analytical approach, the effect of different parameters, including the wall rotation (ψ) and friction angle (ϕ), on the lateral earth pressure can be investigated. Also, in order to study the accuracy of the proposed model just established, the experimental results are also included.

6.1 EFFECT OF WALL ROTATION ON THE PASSIVE PRESSURE

To investigate the effect of the wall rotation, the passive pressure escalation was calculated, using the analytical model. The results that are presented in Fig. 10 are for ϕ=32.5º. Also included in this figure, are the experimental results for the first cycle of movement (the initial friction angle). This also helped to evaluate the accuracy of the proposed analytical model. For this purpose, the maximum movements of the top wall including $(d/2)_{max}$=1.75, 2.45 and 6.50 mm, equivalent to the wall rotation of ψ=0.143º, 0.201º and 0.532º, were considered.

The following observations are based on this figure:

- With increasing wall rotation, the magnitude of the passive pressure on the top of the wall increases, but the passive pressure in the bottom part and near the hinges decreases. Also, the location of the maximum pressure moves gradually from the top of the wall towards the lower region.
- Since the stress in the hinge decreases due to the arching phenomenon between the materials and the wall, it is concluded that by increasing the rotation of the wall, the arching effect increases in the bottom parts.
- Since the maximum pressure location separates the place of the upper and the lower parts of the wall, it can be deduced that by increasing the rotation wall, the height of the arch zone has been decreased. In other words, by increasing the rotation of the wall, the plastic deformation increases in the upper part and the height of the arch zone moves down.

6.2 THE EFFECT OF THE NUMBER OF CYCLES ON THE PASSIVE PRESSURE

Generally, when granular material is subjected to cyclic displacement, especially for loose and medium dense sand, the sand void decreases and it becomes increasingly dense, i.e., it tends to reach the densest possible state. This in turn results in an increase in the material friction angle during successive cycles [1, 20]. This fact was also observed for the sand just adjacent to the wall, which resulted in a markedly settlement in the upper region (see Fig. 6).

Now, based on the analytical model and by considering different angles of friction, the amount of passive

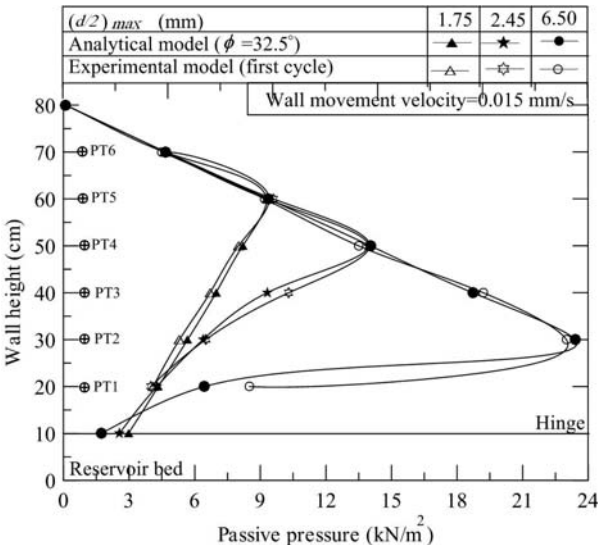

Figure 10. The effect of different wall rotations on the passive pressure escalation.

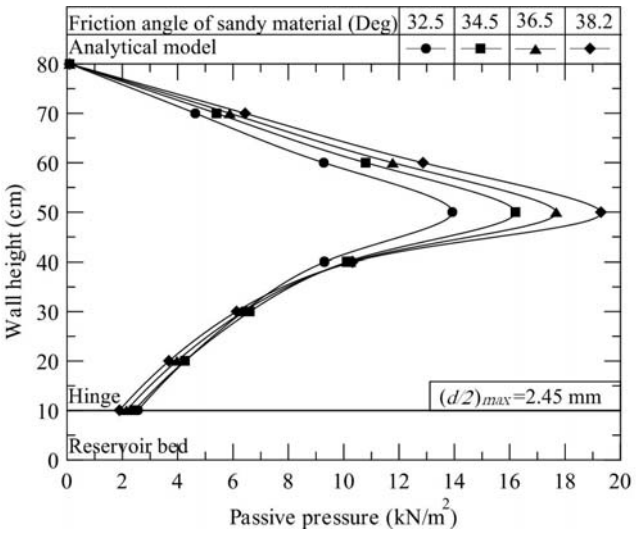

Figure 11. Calculation of the lateral passive pressure on the wall based on the analytical model.

pressure on the wall can be calculated. For example, for a $(d/2)_{max}$=2.45 mm, equivalent to the wall rotation of ψ=0.201° and different friction angles (for example, ϕ=32.5, 34.5, 36.5 and 38.2°), the passive earth pressure was calculated and shown in Fig. 11.

Since the initial angle of friction (ϕ_{ini} =32.5º) and the final angle of friction (ϕ_{max} =38.2º) is known (Table 1) the analytical model has been established for these values of ϕ. The results of the model together with the experimental results for the first and the 50th cycle (for which no significant change in pressure is observed) are compared in Fig. 12. The same result has been observed between the analytical model and the experimental results.

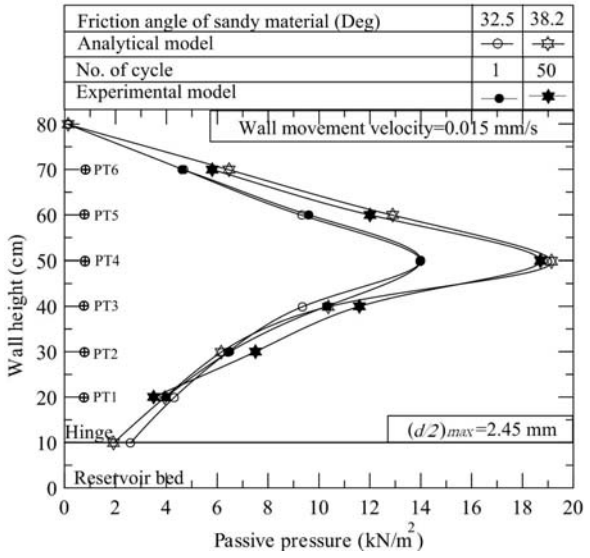

Figure 12. Comparison of tests results with analytical relations in the displacement range 2.45 mm.

In addition, it can be deduced that by increasing the number of cycles, the maximum magnitude of the passive pressure on the wall increases. The passive pressure, however, decreases in the lower part of the wall, which is due to the strengthening of the arch.

7 CONCLUSION

The present research focuses on evaluating the interaction between the soil and the rigid wall in large rotations. A model retaining wall apparatus was designed and constructed. In addition, an analytical model provided to imitate the cyclic behaviour of the granular material behind the rigid wall. For practical purposes and loose sand, the wall displacements considered in this study were d/2=1.75, 2.45 and 6.50 mm. The most important points in this research are as follows:

- The distribution regime of the passive pressure is nonlinear. The passive pressure increases with depth, reaches a maximum, after which it decreases in the lower part of the wall.
- With an increase in the wall rotation amplitude, not only the amount of maximum pressure on the wall increases, but its location also moves gradually downwards. In other words, the plastic zone increases and the height of the arched zone decreases.
- For a specific wall rotation, as the number of cycles increases, the maximum passive pressure increases. After a limited number of cycles, the magnitude of the passive pressure remains roughly constant and no significant variation can be observed.
- In the lower part of the wall, by increasing the wall rotation amplitude and the number of cycles, the passive pressure tends to reduce. This is due to the increasing arch effect.
- It can be deduced that the magnitude of the passive pressure is not constant and depends on the magnitude of the wall rotation. In practice, it is not convenient to use the Coulomb theory for a lateral earth evaluation.

REFERENCES

[1] Xu, M., Clayton, C.R., and Bloodworth, A.G. (2007). The earth pressure behind full-height frame integral abutments supporting granular fill. *Canadian Geotechnical Journal*, Vol. 44, No. 3, pp. 284-298.

[2] Ahn, J.-H., Yoon, J.-H., Kim, J.-H., and Kim, S.-H. (2011). Evaluation on the behavior of abutment-pile connection in integral abutment bridge. *Journal of Constructional Steel Research*, Vol. 67, No. 7, pp. 1134-1148.

[3] Dicleli, M. and Erhan, S. (2010). Effect of soil-bridge interaction on the magnitude of internal forces in integral abutment bridge components due to live load effects. *Engineering Structures*, Vol. 32, No. 1, pp. 129-145.

[4] Hassiotis, S. and Xiong, K. (2007). Field measurements of passive pressures behind an integral abutment bridge. *Proceedings of the 7th International Symposium on Field Measurements in Geomechanics, Boston, MA, United states, American Society of Civil Engineers.*

[5] Khodair, Y.A. and Hassiotis, S. (2005). Analysis of soil-pile interaction in integral abutment. *Journal of Computers and Geotechnics*, Vol. 32, No. 3, pp. 201-209.

[6] Noorzaei, J., Abdulrazeg, A.A., Jaafar, M.S. and Kohnehpooshi, O. (2010). Non-linear analysis of an integral bridge. *Journal of Civil Engineering and Management*, Vol. 16, No. 3, pp. 387 - 394.

[7] Charuchaimontri, T., Senjuntichai, T., Ožbolt, J. and Limsuwan, E .(2008). Effect of lap reinforcement in link slabs of highway bridges. *Engineering Structures*, Vol. 30, No. 2, pp. 546-560.

[8] Marques Lima, J. and de Brito, J. (2009). Inspection survey of 150 expansion joints in road bridges. *Engineering Structures*, Vol. 31, No. 5, pp. 1077-1084.

[9] Tsang, N.C.M., England, G.L. and Dunstan, T. (2002). Soil/structure interaction of integral bridge with full height abutments. *Proc 15th ASCE Engineering Mechanics Conference, Columbia University, New York, NY, USA*.

[10] Dicleli, M. (2000). A rational design approach for prestressed-concrete-girder integral bridges. *Engineering Structures*, Vol. 22, No. 3, pp. 230-245.

[11] Alizadeh, M.H., Rashid, A.R.K., Chik, Z. and Mirhosseiny, S.M. (2010). Investigation of Abutment Displacement of a Full Height Integral Bridges in Dense Granule Backfill. *American Journal of Engineering and Applied Sciences*, Vol. 3, No. 4, pp. 749-756.

[12] Barker, K.J. and Carder, D.R. (2001). Performance of an integral bridge over the M1-A1 Link Road at Bramham Crossroads. Transport Research Laboratory, Crowthorne, Berkshire, UK.

[13] Barker, K.J. and Carder, D.R. (2000). Performance of the two integral bridges forming the A62 Manchester road over bridge. Transport Research Laboratory, Crowthorne, Berkshire, UK.

[14] Cosgrove, E. and Lehane, B.H. (2003). Cyclic loading of loose backfill placed adjacent to integral bridge abutments. *International Journal of Physical Modelling in Geotechnics*, Vol. 3, No.3, pp. 9-16.

[15] Darley, P., Carder, D.R. and Barker, K.J. (1998). Seasonal thermal effects over three years on the shallow abutments of an integral bridge in Glasgow. Transport Research Laboratory, Crowthorne, Berkshire, UK.

[16] Goh, D. (2001). The behavior of shallow abutments of integral bridges. PhD Thesis, University of Birmingham, Birmingham.

[17] Movahedifar, M. and Bolouri-Bazaz, J. (2011). An innovative apparatus to measure cyclic behavior of backfill granular material behind bridge abutment. *in The 14th Asian Regional Conference on Soil Mechanics and Geotechnical Engineering, Hong Kong*.

[18] Springman, S.M., Norrish, A.R.M., and Ng, C.W.W. (1996). Cyclic loading of sand behind integral bridge abutment. Transport Research Laboratory

[19] Tapper, L. and Lehane, B.M. (2004). Lateral stress development on integral bridge abutments. *in The Eighteenth Australasian Conference on Mechanics of Structures and Materials, Perth*.

[20] England, G.L. and Bolouri-Bazaz, J. (1995). Ratching flow of granular materials. *Proceeding of Static and Dynamic Properties of Gravelly Soil, AISC, Geotechnical Division*.

[21] Paik, K.H. and Salgado, R. (2003). Estimation of active earth pressure against rigid retaining walls considering arching effects. *Journal of Geotechnique*, Vol. 53, No. 7, pp. 643-653.

[22] Roy, A. and Patra, N.R. (2009). Effect of arching on passive earth pressure for rigid retaining walls considering translation mode. *Proceedings of the 2009 Structures Congress, United states, American Society of Civil Engineers*.

[23] Rupa, S.D. and Pise, P.J. (2008). Effect of arching on passive earth pressure coefficient. *in The 12th International Conference of International Association for Computer Methods and Advances in Geomechanics, Goa, India*.

[24] Phillip, S.K.Ooi, Xiaobin, L. and Harold, S.H. (2010). Numerical Study of an Integral Abutment Bridge Supported on Drilled Shafts. *Journal of Bridge Engineering*, Vol. 15, No. 19, pp. 19-31.

[25] Card, G.B. and Carder, D.R. (1993). A literature review of the geotechnical aspects of integral bridge abutments. Transport Research Laboratory, Crowthorne, Berkshire, UK.

[26] Bayoglu Flener, E. (2004). Soil-Structure interaction for integral bridges and culverts. PhD Thesis, Royal Institue of Technology, Stockholm, Sweden.

[27] Benmebarek, S., Khelifa, T., Benmebarek, N. and Kastner, R. (2008). Numerical evaluation of 3D passive earth pressure coefficients for retaining wall subjected to translation. *Computers and Geotechnics*, Vol. 35, No. 1, pp. 47-60.

[28] Fang, Y.-S., Ho, Y.-C. and Chen, T.-J. (2002). Passive Earth Pressure with Critical State Concept. *Journal of Geotechnical and Geo-environmental Engineering*, ASCE, Vol. 128, No. 8, pp. 651-659.

[29] James, R.G. and Bransby, P.L. (1970). Experimental and theoretical investigations of a passive earth pressure problem. *Journal of Geotechnique*, Vol. 20, No. 1, pp. 17-37.

[30] Matsuzawa, H. and Hazarika, H. (1996). Analyses of active earth pressure against rigid retaining wall

subjected to different modes of movement. *Journal of Soil and Foundations*, Vol. 36, No. 3, pp. 51-65.

[31] Das, B.M. (2002). Principles of foundation engineering. 4th Bill Stenquist, Virginia, USA.